www.czasopisma.pan.pl PAN POLSKA AKADEMIA NAUK www.journals.pan.pl

PAN ARCHIVES OF ACOUSTICS
Vol. 40, No. 4, pp. 527–537 (2015)

DOI: 10.1515/aoa-2015-0052

Electroacoustic Analysis of a Controlled Damping Planar CMOS-MEMS Electrodynamic Microphone

Farès TOUNSI[(1)], Brahim MEZGHANI[(1)], Libor RUFER[(2)], Mohamed MASMOUDI[(1)]

[(1)] *EMC Research Group*
National Engineering School of Sfax, University of Sfax
Route Soukra, BP 1173, 3038 Sfax, Tunisia; e-mail: fares.tounsi@isimsf.rnu.tn

[(2)] *TIMA Laboratory, University Grenoble Alpes*
46, Avenue Félix Viallet, 38031 Grenoble, France

(*received April 8, 2015; accepted September 30, 2015*)

This paper gives a detailed electroacoustic study of a new generation of monolithic CMOS micromachined electrodynamic microphone, made with standard CMOS technology. The monolithic integration of the mechanical sensor with the electronics using a standard CMOS process is respected in the design, which presents the advantage of being inexpensive while having satisfactory performance. The MEMS microphone structure consists mainly of two planar inductors which occupy separate regions on substrate. One inductor is fixed; the other can exercise out-off plane movement. Firstly, we detail the process flow, which is used to fabricate our monolithic microphone. Subsequently, using the analogy between the three different physical domains, a detailed electro-mechanical-acoustic analogical analysis has been performed in order to model both frequency response and sensitivity of the microphone. Finally, we show that the theoretical microphone sensitivity is maximal for a constant vertical position of the diaphragm relative to the substrate, which means the distance between the outer and the inner inductor. The pressure sensitivity, which is found to be of the order of a few tens of μV/Pa, is flat within a bandwidth from 50 Hz to 5 kHz.

Keywords: MEMS sensor, acoustical model, monolithic electroacoustic microphone, suspended diaphragm, lumped element modeling.

1. Introduction

The evolution of integrated circuits technology by the end of the 20th century was dominated by the miniaturization, providing them more functionality and reliability. A diversion of microelectronics led to Microsystems technology (or MEMS – Micro-Electro-Mechanical Systems), which combines semiconductor microelectronics process and micromachining expertise, allowing the realization of complete systems on a chip (Ma, 2015). It was this marriage that gave birth to Microsystems devices, which are supposed to be more "intelligent" by providing them with analytical skills, decision-making and communication ability with the outside environment. The scope of Microsystems is very wide, but certainly, telecommunication sector has the stronger potential of functions. Among successful applications, the micromachined microphone has become a very actively pursued sensor in the last several years, used in many fields such as broadcasting, hearing aids, telecommunications and tape recording (Chen *et al.*, 2008). Since the first silicon micromachined microphone presented in 1983 (Royer *et al.*, 1983), a number of different approaches have emerged including capacitive microphone type, which earned the highest degree of success among all MEMS microphones due to its superior sensitivity, low temperature coefficient and long-term stability in telecommunication and hearing aid devices (Kühnel, Hess, 1992; Kronast *et al.*, 2001). However, its integration with electronics on the same chip needs specific materials and fabrication technologies, which may limit the affordability of these types of microphones and increase the cost.

The electrodynamic (or inductive) microphone, presented in this paper, will overcome this technological handicap and allow a totally monolithic integration of the sensor with its electronics, using standard

CMOS process. An attempt to manufacture a miniaturized electrodynamic microphone was made in the past, however it combined a diaphragm with coils manufactured in MEMS technology, and a macro-magnet embedded in the external package (Horng *et al.*, 2010). Thus, the introduction of the entirely micromachined electrodynamic microphone can solve size and cost issues since it uses standard silicon CMOS fabrication technology. Moreover, our inductive microphone will represent a high linearity since it generates both even and odd-order harmonics and inter-modulation products (Abuelma'atti, 2007). In this approach, we use silicon and other layers issued from a CMOS process as basic structural materials for the mechanical part of the system. The operation mode of the inductive microphone is based on the variation of mutual inductance between a planar external fixed inductor and an internal suspended one.

In Sec. 2, we present the MEMS-based electrodynamic microphone structure as well as its fabrication flow. The electro-acoustic behavior of the complete microphone structure is detailed in Sec. 3. In Sec. 4, we present the microphone frequency response and the sensitivity simulation results. Finally, Sec. 5 summarizes the present work.

2. Description of the microphone and its fabrication process

2.1. Planar CMOS-MEMS electrodynamic microphone structure

The proposed structure of the electrodynamic microphone is shown in Fig. 1 (Tounsi *et al.*, 2009b). The microphone consists mainly of two inductors which occupy separate regions. The first one, a stationary outer inductor L_1, is placed on top of the substrate. The second one, an inner inductor L_2 is implemented on top of a thin plate suspended over a micromachined cavity. The plate is attached to the substrate using four arms, one at each corner (see Fig. 2a) and serves as the microphone diaphragm. The electromagnetic field necessary for the microphone operation can be produced by an electrical bias applied in one or in

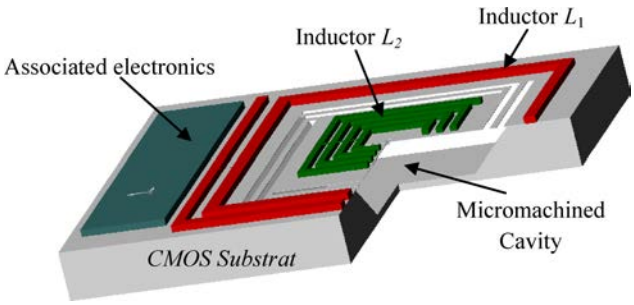

Fig. 1. Structure of the planar CMOS-MEMS electrodynamic microphone.

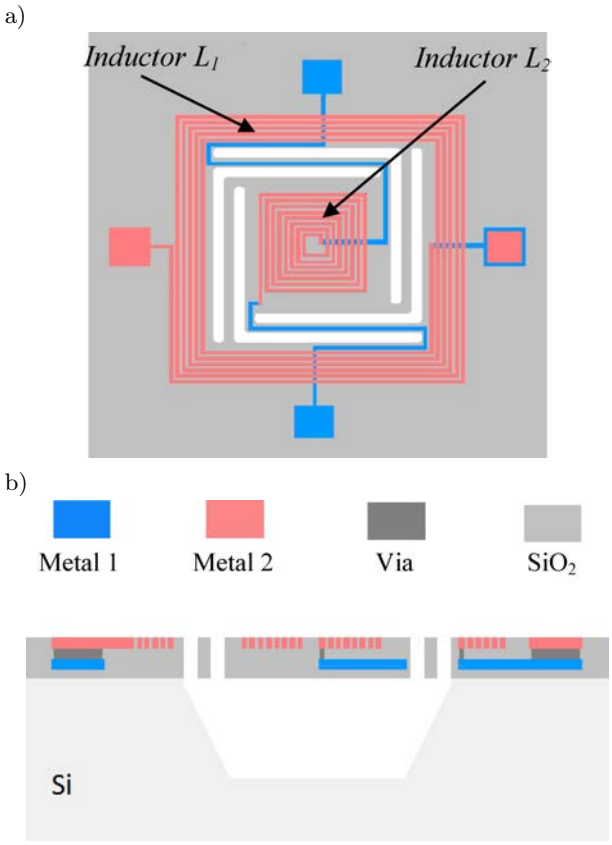

Fig. 2. A layout showing both inductors used in the electrodynamic microphone in a) top view, b) cross-section.

both inductors. The bias can be insured either with a direct current (*DC*) or with an alternating current (*AC*). Thus, a magnetic field variable in space and/or in time will be generated in the vicinity of the inner inductor L_2. When an AC biasing is applied, an additional voltage component, named transforming induction, will be induced leading to an increasing of the total voltage magnitude to the detriment of the front-end electronics, which should include an amplitude modulation/demodulation (Tounsi *et al.*, 2009a; Tounsi, 2013). In response to an incident acoustic energy, the suspended diaphragm will vibrate causing a movement of L_2. According to Faraday's law, the vibration of L_2 within a magnetic field will generate, at its ends, an electromotive force (*emf*), proportional to the amplitude of the incident acoustic pressure. The resulting voltage will be processed by the electronic circuitry integrated on a same chip. This monolithic integration will increase performances, miniaturize the system, increase the sensitivity and in particular decrease the noise, due to the reduction of interconnections parasitic capacitance. Furthermore, this approach focuses on low-cost MEMS microphone obtained by processing chips issued from an industrial standard 0.35 µm CMOS process. The cavity under the suspended diaphragm could be fabricated using bulk micromachin-

ing etching, which is compatible with the standard CMOS process.

Because of the simple layout and symmetry properties of the square geometry, both internal and external spiral inductors will have a squared form. Figure 2a shows a simplified layout of both inductors, having only 5 turns as an example. Several metallic layers can be available in CMOS technology. In our case, the planar inductor is formed with the upper metallic layer (Metal 2, in Fig. 2b) to reduce the parasitic capacitance. Often, the upper metallic layer is thicker than the other layers, thereby minimizing the static series resistance of the inductor. The inner end of the inner inductor is connected by the means of "via" connections with the lower metal layer (Metal 1, as shown in Fig. 2a). The geometric parameters of the inductor pattern (such as spire width, spire spacing, outer and inner effective diameter, number of turns and the inductor shape) are controlled by the desired performances; whereas technological parameters (such as metal conductivity, substrate resistivity, oxide thickness and metal thickness) are fixed by the given CMOS technology.

2.2. Fabrication process of the electrodynamic microphone

The fabrication process of the acoustic sensor is based on a CMOS compatible process followed by an additional bulk micromachining post-process to release both diaphragm and its attachments (Kovacs *et al.*, 1998). We show in Fig. 3 the fabrication process flow of the sensitive part of the sensor (inductors and diaphragm) using steps of CMOS electronics manufacturing for the inductors deposition combined with a post-process used for the diaphragm release. Figure 3a shows a silicon wafer, on which a first dielectric layer of SiO_2 is deposited and opened by lithography in predefined locations. Thereafter, the contact lines for both inductors are deposited in Metal 1 layer. This step is followed by a dielectric material layer (SiO_2) deposition on the entire surface of the chip (see Fig. 3b). There is not detailed the location and the geometry of openings in dielectric and passivation layers to expose the silicon substrate to the etching post-process step. These openings are placed in appropriate locations to obtain an exposed silicon surface and subsequently allow the diaphragm release. In the next step a layer is deposited in Metal 2 to create both inductors L_1 and L_2 and contact pads (Fig. 3c). Next, a final silicon nitride layer is deposited on the inductor as a passivation layer to protect the circuit surface and the processing electronics (Fig. 3c). After the chip fabrication, the final stage is a post-process etching step. It involves a TMAH wet etch that attacks only the bulk silicon and subsequently allows the etching of the cavity under the diaphragm. The final cross-sectional view of

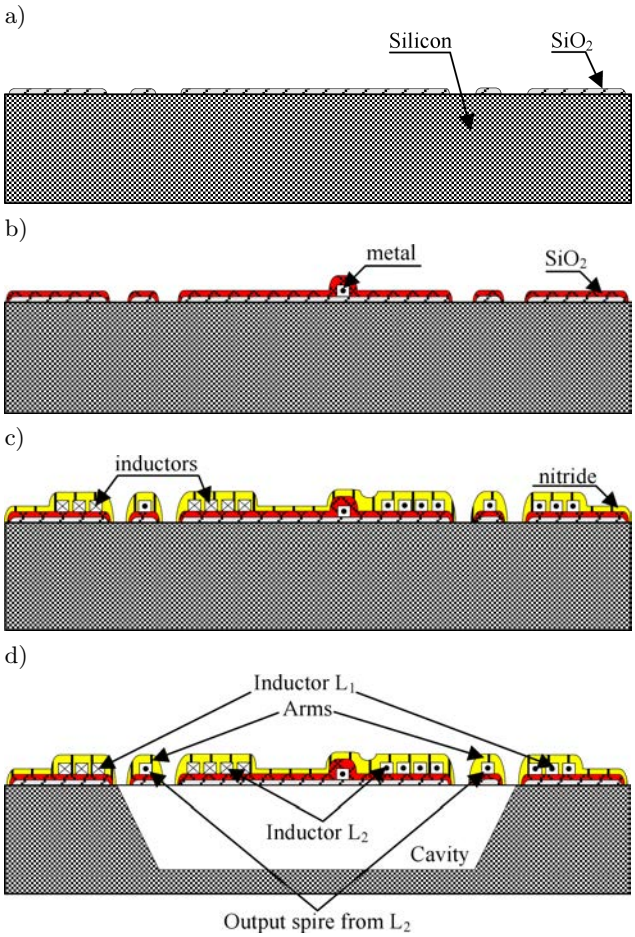

Fig. 3. Fabrication process flow of the planar CMOS-MEMS microphone.

the microphone and the full sequence of layers used in a standard manufacturing process of CMOS ICs are shown in Fig. 3d.

The overall performance of the microphone depends on the size of the suspended diaphragm and is also influenced by the built-in stress. Other parameters, such as the bias voltage and the cavity size, also affect the sensitivity. This is why the microphone must be well dimensioned through an electro-acoustic modeling study, which is the goal of the following section. The induced voltage will be amplified and treated using the nearby electronics monolithically integrated on the same chip.

3. Lumped element modeling of the microphone structure

An electroacoustic transducer is a system that converts the acoustic energy to the electrical energy, and vice-versa. In the case of a microphone, the input signal is transferred from the acoustic domain through the mechanical domain (diaphragm deformation) to reach the electrical domain (variation of the B-magnetic field

leading to the induced voltage in our case). The study of the electroacoustic transducers is commonly performed using lumped element models reflecting electrical, mechanical and acoustic behaviours of the system, which is also the purpose of following subsections (Olson, 1976; Beranek, 1954). This approach remains valid if the smallest acoustic wavelength in the considered frequency range ($f = 20$ kHz, $\lambda = 17$ mm) remains sufficiently high compared to the microphone dimensions. In the opposite case, the interaction between the diaphragm and the sound field may cause sound diffraction, which obviously will introduce errors in the sensor frequency response (Blackstock, 2000).

3.1. Basis of the electro-acoustic modeling

To derive a lumped element model equivalent to a physical device excited by mechanical, acoustic or electromagnetic phenomena, an analogy between different involved physical domains should be used. This will ease the solution of mechanical and/or acoustic systems through converting these coupled problems to the electrical domain and then solving the resulting electrical analog model using classical circuit theory. Acoustic elements encountered in physical devices involve resistances, masses or compliances, according to the behaviour of the device's part in response to an acoustic flow. In our model, the acoustic pressure corresponds to a voltage; an acoustic flow corresponds to a current and volume displacement to an electrical charge. When applying analogy between different energy fields, a lumped element model of the microphone can be built. The analogy requires putting in series all elements crossed by the same acoustic flow and putting in parallel elements corresponding to a flow addition. Lumped element modeling can determine the transducer characteristics as sensitivity, frequency response (particularly amplitude and phase), complex acoustic impedance of the diaphragm, electrical equivalent impedance and the intrinsic electrical noise of the microphone. Moreover, the introduction of transformers allows gathering different domains in the same linear circuit (Blackstock, 2000). The derived diagram of a mechanical-acoustic system always comes down to that of Fig. 4, in which the ideal transformer models the mechanical-acoustic coupling. In this case, the coupling is managed by the pair of equations $F = pS$ and $v = -q/S$ (Beranek, 1954). In practice, a transformer is always accompanied by impedance at its input and output ports (see Fig. 4b). In the microphone system, the mechanical part is modeled by a source of a strength F and impedance Z_m, on the other hand, the acoustic part by a source of strength p and impedance Z_a. The circuit, shown in Fig. 4c, is the acoustic equivalent of that of Fig. 4b with the impedance and the force transferred from the

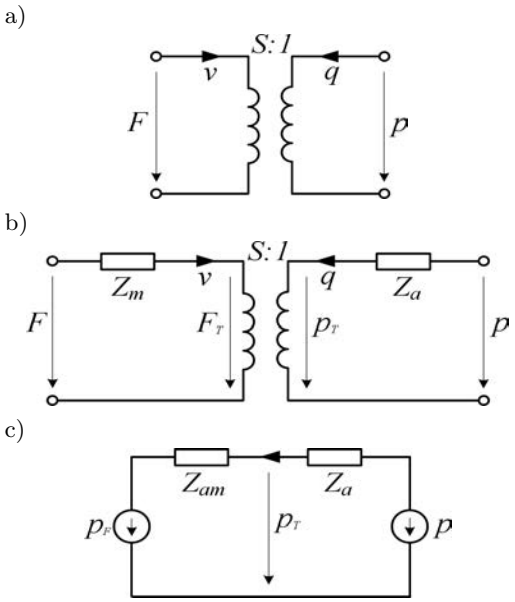

Fig. 4. Representation of the mechanical-acoustic coupling in the form of a) transformer between the two domains, b) coupling scheme, c) equivalent acoustic scheme.

primary to the secondary winding, so avoiding using a transformer. Thus, the equivalent impedance and pressure are given by $Z_{am} = Z_m/S^2$ and $p_F = F/S$, respectively.

3.2. Microphone equivalent electro-acoustic circuit

The electrodynamic microphone structure can be simplified by a symbolic mechanical-acoustic circuit given in Fig. 5a. It consists of a suspended diaphragm, which separates the back chamber from the front space, attached by four arms playing a role of mechanical springs. We consider, as the only possible movement, a vertical harmonic oscillation around its equilibrium (or rest) position, which progressively damps until it stops. This damping comes, on one hand, from the acoustic radiation and the reaction forces of the environment opposing to the movement, and, on the other hand, from the energy losses by internal friction in the suspension. The electroacoustic lumped equivalent model, shown in Fig. 5b, essentially consists of five components: {1} the radiation impedance, M_{rad} and R_{rad}, generated by the diaphragm movement, {2} the diaphragm impedance itself, M_{mem} and C_{mem}, {3} the impedance of holes around the diaphragm attachment arms, M_{open} and R_{open}, and {4} the acoustic compliance of the cavity beneath the diaphragm, C_{back}. In our electroacoustic model, the voltage is represented by the sound pressure acting on the diaphragm, $p_{in}(t)$, and the current is represented through the acoustic flow, $q(t)$. Subsequently, an explanation of each equivalent circuit element is detailed.

a)

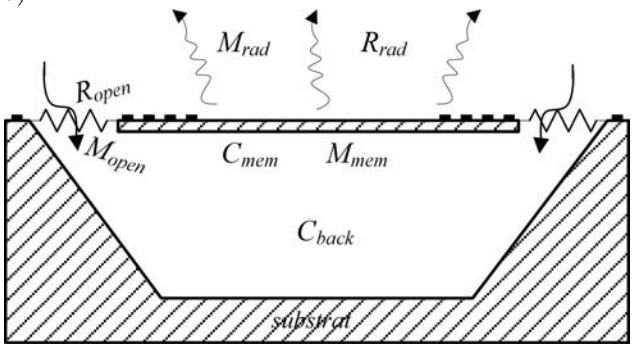

b)

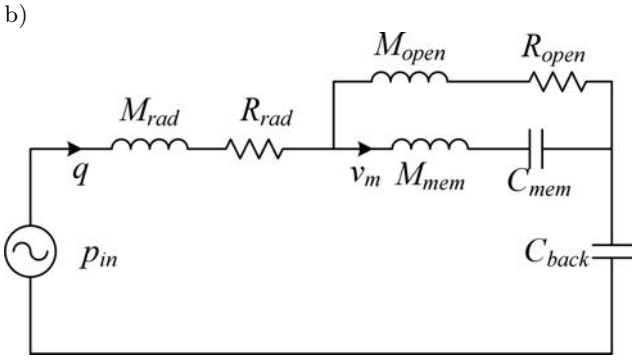

Fig. 5. a) The symbolic mechanical-acoustic circuit, b) the equivalent lumped element model of the electrodynamic microphone structure.

3.2.1. Radiation impedance

The front of the electroacoustic transducer is comprised of a suspended square diaphragm, flat, thin and sufficiently rigid, attached to the substrate by four arms. For small diaphragm dimensions, compared to the wavelength λ, the phase effect and diffraction become negligible and the force developed by the pressure does not depend on the incidence angle (omnidirectional microphone). We can consider that the diaphragm behaves as a rigid piston with active surface S (Rossi, 2007). When the diaphragm vibrates in response to a sound pressure, a sound wave is generated in contact with the air particles and radiates outward, it acts as a speaker (Baltes *et al.*, 2005). This mechanism may be important if the length of the acoustic wave is less than or equal to a certain dimension of the mechanical element, which is rare in MEMS. A radiation of a rigid piston is represented by mechanical radiation impedance, Z_{rad}, consisting of a radiation mass, M_{rad}, and a radiation resistance, R_{rad}. This mechanical impedance is given for a square piston by (Morse and Ingard, 1968):

$$\underline{Z^{me}_{rad}} = c_{air}\rho_{air}\left[\theta_0(ka) - j\chi_0(ka)\right], \qquad (1)$$

where j is the unit imaginary number, a is the diaphragm square side, c_{air} is the speed of sound in air, ρ_{air} is the density of air, k is the wave number which is equal to ω/c_{air} (or $2\pi/\lambda$, λ: wavelength), ω is the angular frequency of the incident wave and θ_0 and χ_0 are given by:

$$\theta_0(x) = 1 - \frac{2}{x}J_1(x), \qquad \chi_0(x) = \frac{2}{x}H_1(x), \qquad (2)$$

where J_1 and H_1 are the Bessel functions of the first kind and the Struve function of order one, respectively (Howard, Cazzolato, 2014). By dividing Eq. (1) by S^2 and applying a Fourier series expansion for J_1 and H_1 when $ka \to 0$ gives the following expression:

$$\underline{Z^{ac}_{rad}} = \frac{c_{air}\rho_{air}}{a^2}\left[\frac{1}{8}(ka)^2 - j\frac{4}{3}\frac{ka}{\pi}\right]$$

$$= \frac{1}{8}\frac{\rho_{air}}{c_{air}}\omega^2 - j\frac{4}{3\pi}\frac{\rho_{air}}{a}\omega = R_{rad} + j\omega M_{rad}. \qquad (3)$$

The acoustic radiation impedance can be viewed as a sum of an acoustic resistance plus an acoustic mass. The negative sign in the expression of M_r indicates that towards low frequencies, the air particle velocity is in a phase lead of 90° with respect to pressure.

3.2.2. Impedance of the diaphragm and attachment arms

In the electrodynamic microphone structure, the diaphragm and its attachment arms represent a mechanical resonator, which is a key element in the acoustic-mechanical transduction scheme. If we can assume that the diaphragm can vibrate without deformation and it is not limited by a damping, it can be considered as a piston with a mass m and an active surface S, attached with a substrate through arms with a spring constant (stiffness) of k. The total mechanical impedance is then given by the sum of the impedances of the diaphragm and of the attachment arms. The vibration of the diaphragm attachment arm is modeled by the mechanical impedance composed of its reduced mass and an ideal compliance C_{mem}. The value of the arms compliance, C_{mem}, is inversely proportional to their mechanical stiffness, k_{zz}. Several stiffness types are studied and their expressions are given in a previous paper (Tounsi *et al.*, 2009b). The second term, constituting the system mass, is the sum of both, diaphragm and arms equivalent masses, considered in harmonic vibration. Therefore, the total mechanical impedance of the system is expressed as:

$$\underline{Z^{me}_{mem}} = j\omega(M_{mem} + M_{arms}) + \frac{1}{j\omega C_{mem}}. \qquad (4)$$

By converting Eq. (4) from the mechanical to the acoustic domain, the acoustic impedance of the diaphragm with four attachment arms can be obtained by dividing the mechanical impedance by S^2. The equivalent mass of each arm, in harmonic vibration mode, is expressed by the concept of reduced mass.

The reduced mass of a beam clamped at one side, with respect to the anchor, can be calculated, through a simplified approach, by multiplying the real mass by the coefficient 0.236 (Mir *et al.*, 2002), so the total acoustical impedance will be approximated by the following equation:

$$\underline{Z^{ac}_{mem}} = j\omega\frac{\rho_0}{a^2}\left(t + 4\cdot 0.236\frac{tw_b}{a}\right) + \frac{k_{zz}}{j\omega a^4}, \quad (5)$$

where ρ_0 and t are the average density and the equivalent thickness, respectively, of the materials forming the diaphragm (or the arm) and w_b is the width of the arm.

3.2.3. Impedance of diaphragm openings

It is necessary, for microphone operation, to consider two types of slots. Firstly, the slots delimited by the attachment arms and the substrate are found on all four sides of the diaphragm. These arms are used not only to fix the suspended diaphragm to the substrate but also to provide additional flexibility to this diaphragm. Secondly, the openings, which are placed at the middle of the diaphragm, are used to facilitate the penetration of the etching solution below the diaphragm during the micromachining of the bulk silicon. A detailed explanation and the analysis of the selected locations and openings number, both around the diaphragm and those at its middle part, can be found in (Tounsi *et al.*, 2009b). If the airflow through the diaphragm openings can be assumed to be incompressible, the openings can be described by complex acoustic impedance. Neglecting the end correction, this impedance, Z^{ac}_{open}, can be described by an acoustic resistance in series with a mass and is written as (Rossi, 2007)

$$\underline{Z^{ac}_{open}} = \frac{12\eta_{air}t}{l_h w_h^3} + j\omega\frac{6\rho_{air}t}{5l_h w_h}, \quad (6)$$

where η_{air} and ρ_{air} are, respectively, the air viscosity and density coefficient at 20°C and l_h and w_h denote the length and width of an opening, respectively. A slot, or opening, is considered as narrow if its width is less than $0.003/\sqrt{f}$ (Rossi, 2007). The transit of sound waves in a narrow slit is influenced predominantly by the acoustic resistance, which is due to the viscosity of air.

Since the incident acoustic flow will be divided between all openings on the diaphragm surface, their equivalent impedances should be placed in parallel within the electro-acoustic model. If the size of each opening is equal, the total opening impedance is obtained if Z_{open} is divided by the total number of openings located on the diaphragm surface.

3.2.4. Acoustic impedance of a cavity

When the air volume in the cavity under the diaphragm, which is closed at its end, is compressible, it can be assimilated to either an acoustic compliance or a resistance. The compliance consideration is valid if its side is bounded by $0.05\sqrt{\pi/f}$ and $10\sqrt{\pi}/f$ (Rossi, 2007). Assuming no significant flow is present in the back cavity and the air is a perfect gas, the impedance of the acoustic compliance is given by the following equation (Rossi, 2007):

$$\underline{Z^{ac}_{back}} = \frac{\rho_{air}c^2_{air}}{j\omega V}, \quad (7)$$

where V is the volume of the back cavity which equivalent mass is neglected in our model. So, in the case when the depth of silicon bulk micromachining is comparable to the diaphragm size, the cavity is modeled by an air chamber. Otherwise, when the etching depth is small, a viscous damping is produced via the air film compression trapped between the diaphragm and the cavity base. This viscous squeeze film damping arises from the interaction of the air with a mechanical structure in motion. Like all surface phenomena, it has a much greater influence on the microscopic scale than in the macroscopic scale. Thus, in the case of a microstructure moving perpendicular to the substrate (see Fig. 6), we commonly use the Reynolds equation to determine the damping forces (Bao, 2000). This general equation, which describes the thin gas compression phenomena, is expressed as follows:

$$\frac{\partial}{\partial x}\left(\rho G^3\frac{\partial p}{\partial x}\right) + \frac{\partial}{\partial y}\left(\rho G^3\frac{\partial p}{\partial y}\right) = 12\eta\frac{\partial(\rho G)}{\partial t}, \quad (8)$$

where p is the ambient pressure variation, p_0 the reference pressure of the undisturbed fluid, η the fluid viscosity, ρ its density and G is the instantaneous height of the air gap. To linearize and also simplify the Reynolds equation, several hypotheses are considered such as a small displacement (relative to the air gap), small changes in pressure (with respect to the reference pressure), rigidity of the structure, etc. Finally, for two rectangular plates of length L and width B, which are not perforated, the mechanical damping coefficient can be given by (Bao, 2005):

$$b_{rec} = \frac{\eta_{air}LB^3}{G_0^3}\beta\left(\frac{B}{L}\right), \quad (9)$$

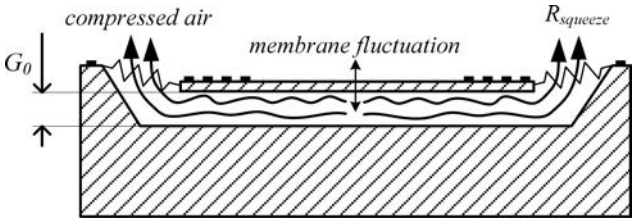

Fig. 6. Illustration of the squeeze film damping occurring through air compression during the diaphragm vertical fluctuation.

where G_0 sets the reference thickness of the air gap around which oscillates the structure and β is a function of B/L ratio, given by (Bao, 2005):

$$\beta\left(\frac{B}{L}\right)=\left\{1-\frac{192}{\pi^5}\left(\frac{B}{L}\right)\sum_{n=1,3,5,..}^{\infty}\frac{1}{n^5}\tanh\left(\frac{n\pi L}{2B}\right)\right\}. \quad (10)$$

For a square diaphragm ($L = B$), the β-function is evaluated to be equal 0.42, and then the acoustic equivalent of the damping coefficient, resulting from the division by S^2, is equivalent to a resistance given by the following equation:

$$R^{ac}_{squeeze} = 0.42\frac{\eta_{air}}{G_0^3}. \quad (11)$$

Table 1 summarizes the acoustic impedances of the various elements in the simulated circuit. The mass of our diaphragm has been evaluated and was found to be equal to 13.4 μg.

Table 1. Values of the electro-acoustic circuit simulated components (when $G_0 = 50$ m).

Equivalent component	Acoustic mass [kg/m^4]	Acoustic resistance [kg/s.m^4]	Acoustic compliance [kg/m^4]
Radiation	364.21	$4.42 \cdot 10^{-4}\ \omega^2$	
Diaphragm	$3.4 \cdot 10^6$		$1.94 \cdot 10^{-11}$
Apertures	167.93	$2.86 \cdot 10^{+9}$	
Cavity		$6.24 \cdot 10^7$	

4. Microphone frequency response and sensitivity

The microphone structure can be, in a first order approximation, simplified as a mass-spring system without damping. This structure has a vibration natural frequency (resonance) equal to $\omega_0 = \sqrt{k/m}$, therefore, the relationship between the vibration amplitude and the system frequency has a peak at ω_0 (Fig. 7). In order to broaden the system bandwidth around its resonance frequency, the vibration amplitude must be attenuated using an energy dissipation mechanism (damping effect). An optimum damping is found as a trade-off between the constant vibration amplitude bandwidth and level (Bao, 2005).

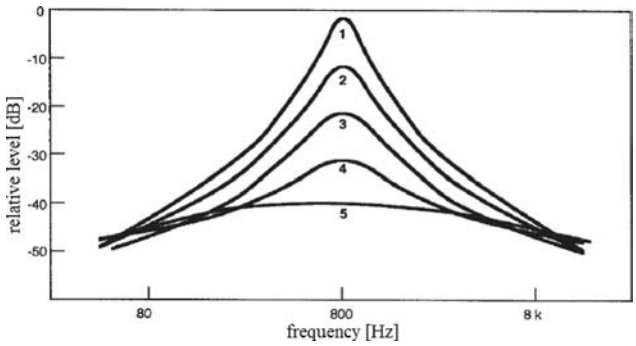

Fig. 7. Frequency response of the diaphragm displacement of a case of the electrodynamic microphone with the effect of an external damping (curves 1 to 5).

4.1. Theoretical frequency response of the microphone

Generally, transduction mechanisms considered for a pressure microphone design exploit either electrical or magnetic fields. The choice of one of these two families of transduction defines the microphone behaviour in the frequency domain. The microphone sensitivity is proportional to the diaphragm displacement when the electrical field is used for electromechanical transduction (capacitive or piezoelectric principle); the term of "displacement microphone" is often used to name this family. If the microphone transduction effect is based on the magnetic field (electromagnetic or electrodynamic principle), the sensitivity is then proportional to the diaphragm velocity, and we call the corresponding family as "velocity microphone". This difference must be taken into consideration when designing the vibration system and considering its resonant frequency. In the case of capacitive microphone, the resonant frequency coincides with the high cutoff frequency. The electrostatic microphone is designed to operate at the frequency range lower than the resonant frequency where its constant frequency response is controlled by the rigidity. For microphones using a magnetic field, the resonant frequency is located at the center of the useful frequency range of the microphone (Merhaut, 1981). Accordingly, the resonant frequency, of these microphones, is substantially lower than that used in the capacitive counterparts. This requirement can be met using either a heavier mass or a smaller spring constant. The electrodynamic microphone is designed to operate at the frequency band around the resonant frequency where its constant frequency response is controlled by the resistance.

Therefore, the electrostatic microphone is designed to operate at its controlled constant rigidity band. Unlike the electrodynamic microphone, that is designed with a damping, which must be constant throughout the useful frequency band. Therefore, displacement microphones are controlled through their compliance, while the velocity microphones are controlled through their resistance. Figure 7 shows, as an example, the diaphragm relative velocity with low damping (in curve 1) along with the effect of an increased damping (in curves 2–5). Notice that since the damping increases, the output at the mid-band becomes increasingly flat, but at the expense of the sensitivity. To achieve a satisfactory frequency response while keeping a good overall sensitivity, several design techniques can be employed. The diaphragm is damped in the case of a conventional electrodynamic microphone

by placing a thin layer of silk (or felt) in the opening between the coil and the air chamber in the rear. In general, the resonant peak is reduced by about 25 to 35 dB, producing the response shown by the curve 5. Adding other damping in mid frequencies by the same method may cause unsatisfactory sensitivity in the system output.

The microphone sensitivity is defined by the ratio between the output voltage and the incident sound pressure on the diaphragm top surface (Gong, 2004). For most applications, the sensitivity of the microphone must be relatively flat and independent of the incident wave frequency. As it was already explained, two kinds of microphones can be distinguished, namely: {i} velocity type (resistive controlled) or {ii} displacement type (compliance controlled). Indeed, as the diaphragm velocity v_m, is inversely proportional to the total impedance of the equivalent acoustic circuit ($v_m \sim 1/Z_{equ}$) for a velocity microphone type, the requirement to have an independent frequency sensibility within the expected frequency range, leads to the condition that Z_{equ} is purely resistive. Consequently, the resonance peak of the diaphragm and attachment arms must be damped (or controlled) using a resistor. Similarly, knowing that the displacement and velocity are related with the following expression $\xi_m = v_m/j\omega$ leads that Z_{equ} must have a character of a compliance to satisfy the condition for the frequency independent characteristics of the displacement microphone.

In the condenser microphone, the sensitivity is proportional to the distance between the two vibrating plates. Thus, the back diaphragm is often perforated to bring it as close as possible to the top one, in order to reduce the air viscosity effect between them. In our setup, this problem does not arise since the rapprochement to ensure is horizontal instead of vertical. In fact, the average diameters of the two inductors should be as close as possible.

4.2. Microphone sensitivity evaluation

The acoustic equivalent circuit of the microphone structure is achieved by substituting the back cavity impedance with an acoustic resistance, given by Eq. (11). For different G_0-values, the total impedance curves of the equivalent circuit are shown in Fig. 8a, and the diaphragm velocity vibration is shown in Fig. 8b. Curves numbered from 1 to 5 correspond to descending values of G_0, as given in Table 2. We note in our design that the curve of the equivalent impedance shape is almost dominated by the microphone back cavity impedance ($Z^{ac}_{equ} \equiv Z^{ac}_{back}$) for different G_0-values (see Fig. 8a). So, to design a velocity microphone with a frequency independent sensitivity, the Z_{equ} module must be constant along the considered frequency range. In order to achieve this requirement, the diaphragm resonant frequency, f_0, should be firstly

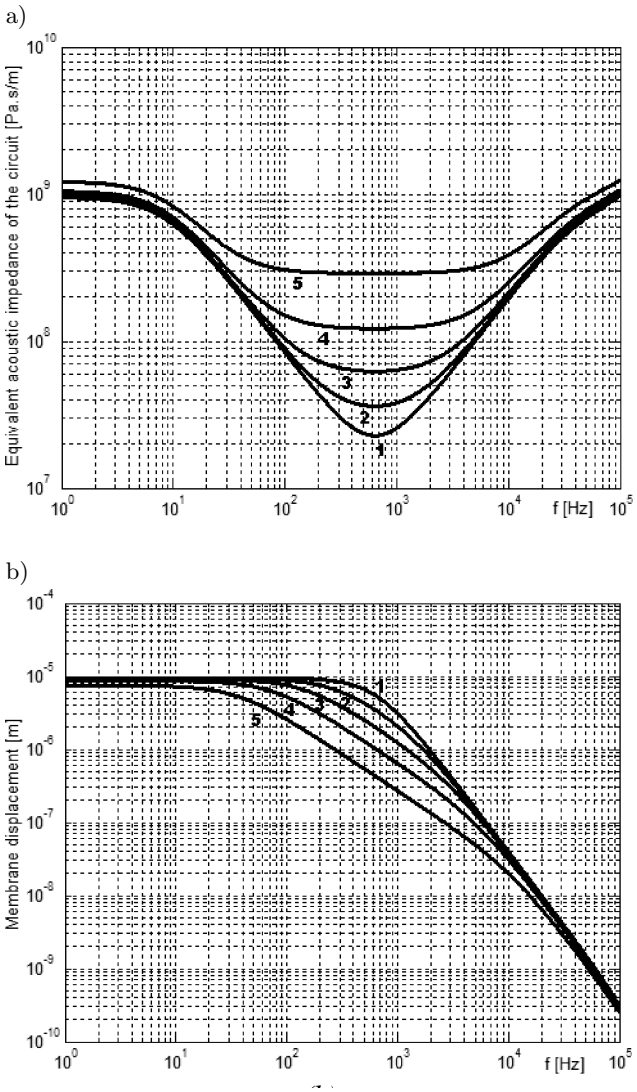

Fig. 8. Shape of the a) acoustic equivalent impedance, b) diaphragm displacement depending on the incident wave frequency for different G_0-values.

Table 2. Evaluated microphone sensitivity and bandwidth values according to air gap thickness.

Air gap thickness G_0 [μm]	Sensitivity S [μV/Pa]	Bandwidth [Hz]
70	> 41.1	286–1.48k
60	> 26.37	210–2.01k
50	> 21.11	134–3.15k
40	> 7.81	74–5.5k
30	> 3.3	37–10.85k

adjusted to the bandwidth geometric center, and secondly, damped using a resistive effect. Thereafter, it is necessary to vary the acoustic resistance value in order to damp the diaphragm vibration around the resonant frequency (see Fig. 8a) by reducing the depth

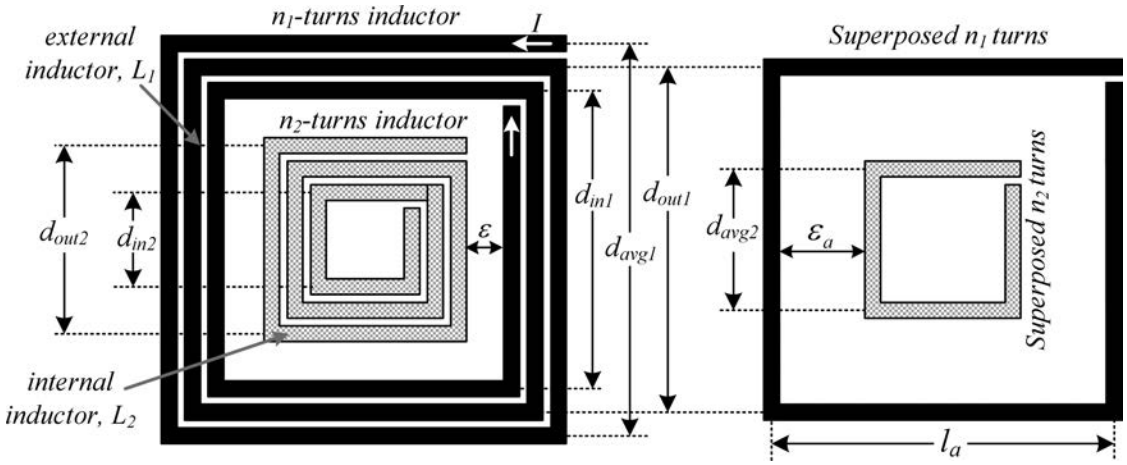

Fig. 9. Considered equivalent scheme of the two inductors (Tounsi, 2013).

of the cavity and subsequently the value of G_0. From the equivalent circuit of the microphone in Fig. 5b, the displacement of the diaphragm is calculated by the following equation:

$$\underline{\xi_m} = \frac{p_{in}}{j\omega \underline{Z^{ac}_{equ}}\, S} \frac{\underline{Z^{ac}_{open}}}{\underline{Z^{ac}_{open}} + \underline{Z^{ac}_{mem}}}. \tag{12}$$

The expression $\underline{Z^{ac}_{open}}/(\underline{Z^{ac}_{open}} + \underline{Z^{ac}_{mem}})$ comes from the fact that the incident wave is divided into two parts, which can be modeled as a current divider: one portion of the wave strikes the diaphragm and the another portion passes through the openings. The diaphragm openings play a similar role as an exhaust vent in capacitive microphones. Their role lies in equalizing the pressure between the back cavity and the atmospheric ambient air, and thus eliminating the effect of the barometric pressure, which leads otherwise to a static deformation of the diaphragm. The impedance value of this equalization hole is chosen such as, within the microphone bandwidth, the flow rate through the hole is negligible.

The microphone velocity curve as a function of the incident wave frequency for different G_0-values is presented in Fig. 10a. So as to achieve flat microphone sensitivity response knowing that the diaphragm performs a constant velocity over the frequency band (see Fig. 10a), we need to use an induced voltage equation which depends only on the velocity. The induced voltage expression is found by evaluating the mutual inductance expression between the two inductors L_1 and L_2, we adopted an approach that consists of replacing both of them by two single turns formed by n_1 superposed spirals for the first and n_2 spirals for the second (see Fig. 9). The side of the resulting spiral is given by the average diameter of the inductors, d_{avg}, of each inductor. Therefore, the output voltage expression that will be used, expressing the cases when only

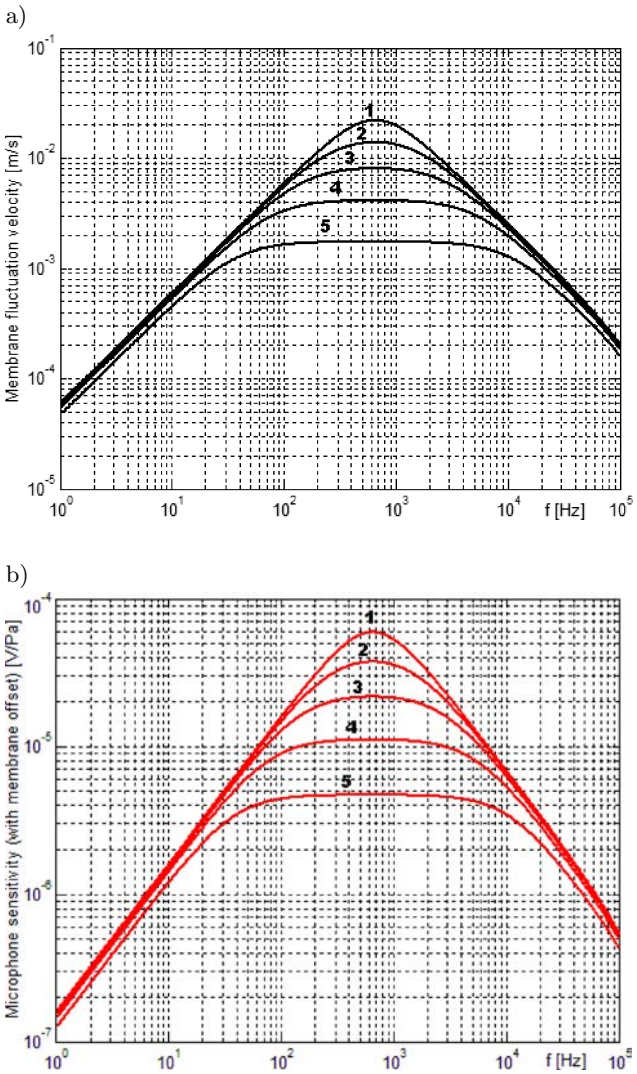

Fig. 10. Shape of the (a) velocity (b) microphone sensitivity as a function of the incident wave frequency for different values of the air-gap thickness G_0 (Curves numbered from 1 to 5 correspond to descending values of G_0, as given in Table 2).

the primary inductor is biased with a DC current I_0 and the diaphragm undergoes a horizontal offset lag, is given by (Tounsi, 2013):

$$V_{off} \approx n_1 n_2 \frac{\mu_0}{\pi}\left(\frac{l_a(l_a-2\varepsilon_a)}{\varepsilon_a\sqrt{8\varepsilon_a^2+l_a^2}}\right) I_0 v_m = B_{\max} I_0 v_m, \tag{13}$$

where ε_a is the average distance between the average inner inductor diameter and outer one and l_a is the average outer inductor diameter, as shown in Fig. 9. It may be noted in this biasing case that the induced voltage is linearly proportional to the rate of change of the diaphragm vibration. In this configuration, the diaphragm must be positioned in advance within a vertical offset where the B-magnetic field is constant and maximum (Tounsi, 2013). Finally, the microphone sensitivity is then plotted in Fig. 10b, and its equation is given by the following expression:

$$S = \frac{\Delta V}{\Delta P} = \frac{B_{\max} I_0 \omega \xi_m}{p_{in}}. \tag{14}$$

The microphone sensitivity is mainly determined by the resonant structure, which is governed by the mass and the bending constant, and secondly by the damping which is a function of the air flow between the back chamber and the ambient air. From Fig. 10b, we note that when the air gap thickness increases, the whole circuit sensitivity also increases, but at the expense of bandwidth. In the case of the electrodynamic microphone, the system is over-damped and the damping resistance mainly controls its performance. At the design phase, the resonant frequency is chosen as a center frequency of the useful frequency band. The value of the resonant frequency appears from the resulting sensitivity curve only as a mean value of the low- and high-frequency limits. Therefore, the air gap must be carefully optimized to achieve acceptable and sufficient bandwidth. Table 2 summarizes evaluated microphone sensitivity and bandwidth values for different air gap thicknesses. According to Table 2, sensitivities in the range of tens of μV/Pa can be achieved, as also shown in Fig. 10b. This sensitivity magnitude is comparable to that reported in literature for some micromachined piezoresistive and piezoelectric microphones (Sheplak *et al.*, 1998; Horowitz *et al.*, 2007).

In the lower frequency end, the electrodynamic microphone bandwidth is limited in particular by the size of the diaphragm and also the rigidity of the arms, which do not allow the diaphragm to reproduce the wide variations of the sound pressure (low-speed and high elongation). At the upper end of the audible spectrum, the bandwidth degradation is mainly due to the effect of inertia of the diaphragm, which leaves it insensitive to small acoustic variations with low energy (high-speed and low elongation). The choice of microphone design parameters (such as inductor size, diaphragm size, arms flexibility, etc.) cannot afford a faithful conversion in both low and high frequency ends, since theoretically, the diaphragm behaves in an opposite way at each of the frequency extremities. For instance, to allow for a rapid diaphragm oscillation, the elastic attachment arms should be flexible at low frequencies and rigid at high frequencies. Alternatively, the diaphragm must be lightweight and therefore have a reduced size at high frequencies, but of considerable length at low frequencies to induce a high power (Faraday's law). The electrodynamic microphone characteristics resulting therefore from a compromise, and must be adapted to the frequency spectrum of the sound signal to transcribe. Thus, for a specific application, both bandwidth and sensitivity should be optimized through a compromise in order to found and achieve the best efficiency.

5. Conclusion

The purpose of this paper is to introduce the design and discuss the electro-mechanical-acoustic behaviour of a new generation of MEMS-based electrodynamic microphone. So, we demonstrated that the operation principle of the monolithic acoustic sensor can be similar to the macroscopic one (traditional). The proposed design is based on two planar spiral inductors and realized using a standard industrial technology completed by a post front side bulk micromachining (FSBM) process. Its operation mode is based on the variation of mutual inductance between an external fixed inductor and an internal suspended inductor. The paper presents the equivalent electrical model describing the microphone acoustic behaviour. The model is built by connecting in parallel components on which same pressure (force) is being applied, and in series components crossed by the same flow (flow velocity). This generated model allows us to estimate the microphone's sensitivity basing on the velocity conversion approach, controlled by a resistance (or damping). The evaluated sensitivity of such a microphone has a value in the range of tens of μV/Pa and has a flat response in the 50 Hz to 5 kHz frequency band. The requirement for this sensitivity, as mentioned previously, is to ensure a diaphragm offset at the location where the magnetic field is at its maximum. In conclusion, we succeeded to have a theoretical flat sensitivity over the entire audio band for a new MEMS-based electrodynamic microphone with a magnitude comparable to that reported in literature for micromachined silicon microphones.

References

1. Abuelma'atti M.T. (2007), *Large signal performance of micromachined silicon inductive microphones*, Journal of Applied Acoustics, **68**, 10, 1286–1296.

2. Baltes H., Brand O., Fedder G.K., Hierold Ch., Korvink J.G., Tabata O. (2005), *CMOS-MEMS: Advanced Micro and Nanosystems*, 1st edition, Wiley-VCH.
3. Bao M.H. (2000), *Micro mechanical transducers: pressure sensors, accelerometers and gyroscopes*, Handbook of Sensors and Actuators, Elsevier, Amsterdam.
4. Bao M. (2005), *Analysis and Design Principles of MEMS Devices*, 1st edition, Elsevier.
5. Beranek L.L. (1954), *Acoustics*, McGraw-Hill Inc, New York, USA.
6. Blackstock D.T. (2000), *Fundamentals of Physical Acoustics*, Wiley, Hoboken, USA.
7. Chen Jen-Yi, Hsu Yu-Chun, Lee Shu-Sheng, Mukherjee Tamal, Fedder Gary K. (2008), *Modeling and simulation of a condenser microphone*, Sensors and Actuators A, 145–146, 224–230.
8. Gong S.C. (2004), *Effects of pressure sensor dimensions on process window of membrane thickness*, Sensor and Actuators A, **112**, 286–290.
9. Horng Ray-Hua, Chen Kuo-Feng, Tsai Yao-Cheng, Suen Cheng-You, Chang Chao-Chih (2010), *Fabrication of a dual-planar-coil dynamic microphone by MEMS techniques*, Journal of Micromechanics and Microengineering, **20**, 1–7.
10. Horowitz S., Nishida T., Cattafesta L. (2007), *Development of a micromachined piezoelectric microphone for aeroacoustics applications*, Journal of Acoustical Society of America, **122**, 3428–3436.
11. Howard C.Q., Cazzolato B.S. (2014), *Acoustic Analyses Using Matlab® and Ansys®*, CRC Press.
12. Kovacs G.T.A., Maluf N.I., Petersen K.E. (1998), *Bulk micromachining of silicon*, Proc. IEEE, **86**, 1536–1551.
13. Kronast W., Muller B., Siedel W., Stoffel A. (2001), *Single chip condenser microphone using porous silicon as sacrificial layer for the air gap*, Sensors and Actuators A, **87**, 188–193.
14. Kühnel W., Hess G. (1992), *Micromachined subminiature condenser microphones in silicon*, Sensors and Actuators A, **32**, 560–564.
15. Ma Ji (2015), *Advanced MEMS-based technologies and displays*, Displays Journal, **37**, 2–10.
16. Merhaut J. (1981), *Theory of Electroacoustics*, McGraw-Hill Inc, USA.
17. Mir S., Charlot B., Rufer L., Parrain F., Martinez S. (2002), *Conception de microsystèmes sur silicium*, Traité EGEM, série Electronique et microélectroniques, Hermes sciences – Lavoisier.
18. Morse P.M., Ingard K.U. (1968), *Theoretical Acoustics*, Chapter 7, 383–394, McGraw-Hill.
19. Olson H.F. (1976), *Acoustical Engineering*, Van Nostrand, Princeton, USA.
20. Rossi M. (2007), *Audio*, Presses polytechniques et universitaires Romande, Italy.
21. Royer M., Holmen J.O., Wurm M.A., Aadland O.S., Glenn M. (1983), *ZnO on Si integrated acoustic sensor*, Sensor and Actuators, **4**, 357–362.
22. Sheplak M., Breuer K.S., Schmidt (1998), *A wafer-bonded, silicon-nitride membrane microphone with dielectrically-isolated single-crystal silicon piezoresistors*, Technical Digest Solid-State Sensor and Actuator Workshop, Transducer Res, Cleveland, USA, 23–26.
23. Tounsi F., Rufer L., Mezghani B., Masmoudi M., Mir S. (2009a), *Electromagnetic Modeling of an Integrated Micromachined Inductive Microphone*, Proceedings of the 4th IEEE International Conference on Design & Test of Integrated Systems in Nanoscale Technology, pp. 1–5, Egypt.
24. Tounsi F., Rufer L., Mezghani B., Masmoudi M., Mir S. (2009b), *Highly Flexible Membrane Systems for Micromachined Microphones – Modeling and Simulation*, Proceedings of the 3rd Int. Conf. on Signals, Circuits and Systems, pp. 1–6, Tunisia.
25. Tounsi F. (2013), *Theoretical Electromagnetic survey: Application to a planar CMOS-MEMS electrodynamics microphone*, [in:] *Novel Advances in Microsystems Technologies and Their Applications*, pp. 205–246, CRC Press, Taylor & Francis.